This is a repository copy of *Neutron radioactivity—Lifetime measurements of neutron-unbound states*.

White Rose Research Online URL for this paper:
https://eprints.whiterose.ac.uk/124734/

Version: Published Version

Article:

Kahlbow, J., Caesar, C., Aumann, T. et al. (4 more authors) (2017) Neutron radioactivity—Lifetime measurements of neutron-unbound states. Nuclear Instruments and Methods in Physics Research, Section A: Accelerators, Spectrometers, Detectors and Associated Equipment. pp. 265-271. ISSN 0168-9002

https://doi.org/10.1016/j.nima.2017.06.002

Neutron radioactivity—Lifetime measurements of neutron-unbound states

J. Kahlbow [a,b,*], C. Caesar [a,b,*], T. Aumann [a,b], V. Panin [c], S. Paschalis [a,1], H. Scheit [a], H. Simon [b]

[a] Institut für Kernphysik, Technische Universität Darmstadt, 64289 Darmstadt, Germany
[b] GSI Helmholtzzentrum für Schwerionenforschung, Planckstraße 1, 64291 Darmstadt, Germany
[c] RIKEN Nishina Center for Accelerator-Based Science, 2-1 Hirosawa, 351-0198, Wako, Saitama, Japan

ABSTRACT

A new technique to measure the lifetime τ of a neutron-radioactive nucleus that decays in-flight via neutron emission is presented and demonstrated utilizing MonteCarlo simulations. The method is based on the production of the neutron-unbound nucleus in a target, which at the same time slows down the produced nucleus and the residual nucleus after (multi-) neutron emission. The spectrum of the velocity difference of neutron(s) and the residual nucleus has a characteristic shape, that allows to extract the lifetime. If the decay happens outside the target there will be a peak in the spectrum, while events where the decay is in the target show a broad flat distribution due to the continuous slowing down of the residual nucleus. The method itself and the analysis procedure are discussed in detail for the specific candidate ^{26}O. A stack of targets with decreasing target thicknesses can expand the measurable lifetime range and improve the sensitivity by increasing the ratio between decays outside and inside the target. The simulations indicate a lower limit of measurable lifetime $\tau \sim 0.2$ ps for the given conditions.

1. Introduction

The access to exotic nuclei opens the possibility to study new kinds of radioactive decays at the limits of nuclear stability (recent reviews, e. g., [1,2]). While for proton-unbound nuclei several cases of "proton radioactivity" have already been measured, no radioactive decay via neutron emission has been observed experimentally yet. This is mainly because the lifetime for proton-unbound nuclei can be rather long ($\sim$ ms) due to the presence of the large Coulomb barrier. For nuclei beyond the neutron drip line, which are candidates for neutron radioactivity, the predicted lifetimes are considerably shorter due to the missing Coulomb barrier. The lifetime is governed mainly by the decay energy and depends strongly on the angular momentum of the decay particles [3], thus reducing the number of possible candidates.

Several definitions of radioactivity are existing, giving different lower limits on the lifetime τ, which marks the boundary between the existence of a nucleus and a ground-state resonance in the continuum, see e. g. [1,4]. Here, $\tau > 10^{-14}$ s will be used as definition of radioactivity, following the guidelines for the discovery of a chemical element from the International Union of Pure and Applied Chemistry (IUPAC) [5].

Fig. 1 shows the different lifetime regimes for radioactivity and resonant phenomena. The new method fills a gap to measure directly lifetimes in the regime of neutron radioactive nuclei.

For the neutron-unbound nuclei with $Z \leq 10$, which can be investigated nowadays, ^{26}O is the most promising candidate. ^{26}O will serve in the following as illustrative example to describe the method. It has been speculated according to the estimates of Grigorenko et al. [3,8], that a very low-lying ground-state resonance of ^{26}O might be rather long-lived representing a case of neutron radioactivity.

Invariant mass measurements of the ^{26}O ground state via proton-removal reaction from ^{27}F have been reported recently by NSCL [9], GSI [6], and RIBF [10] groups. The NSCL and GSI experiments could only deduce upper limits for the energy of the ground state. The experiment performed at RIBF determined the position of the ground-state resonance at $18 \pm 3(\text{stat}) \pm 4(\text{syst})$ keV above neutron-separation threshold, see Fig. 2.

From the GSI data an upper limit of $\tau \leq 5.7$ ns (95% c. l.) for the ^{26}O ground-state lifetime was deduced by the time-of-flight between the target and the spectrometer magnet. The ^{26}O ground-state half-life value of $T_{1/2} = 4.5^{+1.1}_{-1.5}(\text{stat}) \pm 3(\text{sys})$ ps (corresponding to $\tau = 6.5$ ps) has been reported from an analysis of the NSCL measurement [7],
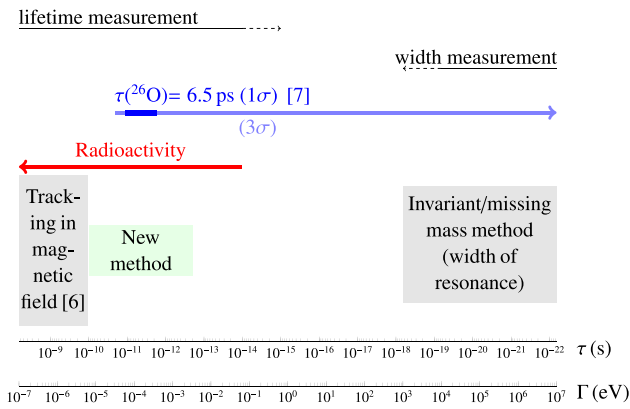
Fig. 1. (Colour online) Characteristic decay widths Γ and corresponding lifetime τ scales are shown. The regimes of radioactive and resonant phenomena are indicated as well as selected experimental techniques that are applicable to measure lifetimes for decays via neutron emission.
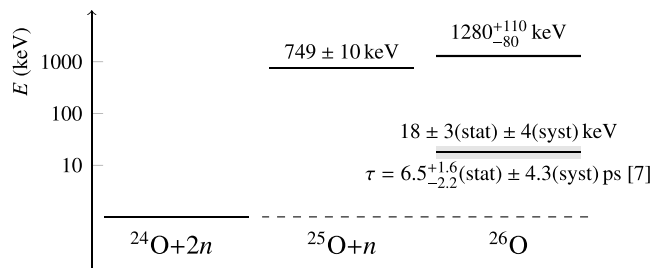

Fig. 2. Excitation energy spectrum of ^{26}O relative to the ^{24}O g. s. in non-linear scale. The values are taken from [10], uncertainty intervals are shown as grey shaded areas. The ground-state decay of ^{26}O via the intermediate ^{25}O resonance is energetically forbidden, the ^{26}O g. s. decays via $2n$ emission to the ^{24}O ground-state.

which, if corroborated, would constitute the first discovery of neutron radioactivity.[2]

Recent theoretical calculations predict that the ^{26}O ground state is dominated by two $d_{3/2}$ valence neutrons [12,13]. Grigorenko et al. [3] state that the influence of pairing and n-n final state interactions and core recoil actually increases the decay width while migrating to lower angular momenta. A precise method to measure lifetimes of neutron-radioactive decays will also help to conclude on the two experimental findings and the theoretical prediction for the ^{26}O ground state, in particular:

- The position of the ground-state resonance [10]; precisely measured to 18 ± 5 keV.
- The experimental lifetime of the ground state [7]; $\tau \leq 11.1$ ps.
- The theoretical relation between the decay energy and the lifetime [3,8], depending on used model interactions.

A direct measurement of the width of the state is impossible because it is much smaller than achievable energy resolutions, which typically are in $\sim$ 10 keV region (cf. Fig. 1), while the width predicted by Grigorenko et al. [3] would only be $\lesssim 10^{-1}$ keV, based on the energy of the experimental ground-state resonance as obtained by Kondo et al. [10].

The technique used by Kohley et al. at NSCL [7,14] is based on a lifetime measurement extracted from the velocity difference measurement of neutrons and the ^{24}O fragment. This velocity difference depends on the energy loss of the charged fragment in the target, causing a shift of the mean velocity difference for finite lifetimes. The method relies

---

[2] Kryger et al. [11] investigated already in 1996 the one-neutron radioactivity of ^{16}B and obtained an upper limit of 191 ps (68% c. l.)

on absolute calibrations of the velocity measurements, which is rather difficult and thus introducing a large systematic uncertainty.

We propose a complementary method, which does not depend on an absolute calibration and is more sensitive. Thus, the method will be able to provide a more precise measurement.

2. Lifetime measurement method

Our method adapts the basic principle of the well known Doppler Shift Attenuation Method (DSAM). In the DSAM [15] nuclear lifetimes of nuclei are measured. The nucleus is formed in an excited state in-flight and slowed down in the target material. While being stopped in the target, the nucleus may emit a γ-ray. The γ-ray energy carries information on the velocity of the emitting nucleus due to the Doppler effect. Taking the stopping power into account allows to extract the decay time of the nucleus.

The new technique presented here to measure lifetimes of possible neutron-radioactive nuclei is based on this idea. The nucleus of interest is produced in-flight at point x_r with reaction cross section σ_r in the reaction target of thickness d, see Fig. 3. The energy loss, which the charged fragment undergoes in the target, depends on the point of decay, which in turn depends on the lifetime of the populated system. The lifetime τ of the nucleus under investigation defines the decay curve:

$$N(t) = N_0 \cdot e^{-t/(\gamma\tau)}, \tag{1}$$

where $N(t)$ is the number of residual nuclei after time t, and $N_0 - N(t)$ the number of products which have decayed already. The time t in the laboratory frame is a function of the travelled straight pathlength x_t and the exponent becomes

$$\frac{x_t}{\beta\gamma c\tau}, \tag{2}$$

let λ be

$$\lambda = \beta\gamma c\tau \tag{3}$$

the decay length with Lorentz factor γ and velocity βc where the velocity is assumed to be constant along the target thickness for the moment. Decays will occur inside and outside the target with amount D_i and D_o, respectively. Considering first the amount of decays inside the target: at the reaction point an amount of initial nuclei dN_0 is produced. The number that decays from there until the end of the target on path $d - x_r$ is, cf. Fig. 3,

$$d\tilde{D}_i = dN_0 \left[1 - e^{-(d-x_r)/\lambda}\right]. \tag{4}$$

Taking into account all the reactions points in the target with cross section σ_r, incoming beam particles N_{in} and target particle-density ρ_t with area density $(dN_0/A)_t = \rho_t \cdot dx_r$ leads to

$$D_i = \int d\tilde{D}_i = \int dN_0 \left[1 - e^{-(d-x_r)/\lambda}\right] \tag{5}$$

$$= \sigma_r \rho_t N_{in} \int_{x_0=0}^{d} \left[1 - e^{-(d-x_r)/\lambda}\right] dx_r \tag{6}$$

$$= \sigma_r \rho_t N_{in} \cdot \left[d - \lambda\left(1 - e^{-d/\lambda}\right)\right]. \tag{7}$$

The amount of decays outside the target D_o is simply the difference between produced nuclei-of-interest in the target and D_i,

$$D_o = \sigma_r \rho_t N_{in} \cdot \lambda \cdot \left[1 - e^{-d/\lambda}\right]. \tag{8}$$

The ratio defined as

$$R(\lambda) = \frac{D_o}{D_i} \tag{9}$$

is

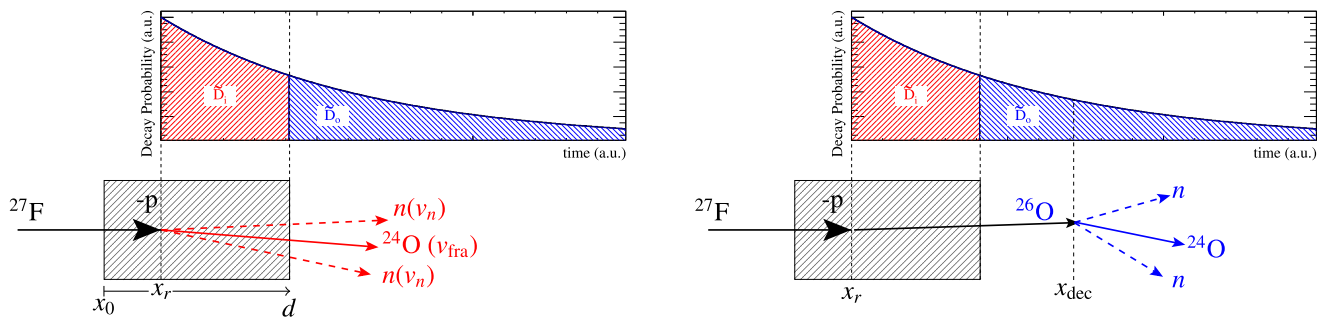$$R(\lambda) = \frac{1}{\frac{d}{\lambda(1-e^{-d/\lambda})} - 1}, \tag{10}$$

Fig. 3. (Colour online) Two event classes appear for an unbound system populated in-flight, which has an appreciable lifetime τ – decays inside and outside the target. An example is shown for proton removal from a ^{27}F beam on a target of thickness d at reaction point x_r and subsequent decay at x_{dec} of the populated ^{26}O into ^{24}O $+ n + n$. Left: An immediate decay inside the target is shown. The amount of decays inside the target from x_r is depicted as $\tilde{D}_i$ (see text). Right: A late decay after the ^{26}O has left the target is displayed, their amount is $\tilde{D}_o$. The velocity difference $\Delta v = v_n - v_{fra}$ (see left Figure) is the parameter of interest.

and depends on the lifetime, $R(\tau)$ with $\tau = \lambda/(\beta\gamma c)$. The decays can be measured and could be disentangled to inside and outside contributions to deduce the lifetime τ. This analytical form of $R(\tau)$ does not include all the physics as, e.g., the stopping power and the resulting effect on β and γ and thus will not be used in the analysis here. It reproduces the behaviour of R as function of τ well for one target, see Fig. 7(b), but shows deviations for consecutive calculations and longer lifetimes as described later. This is one reason why the simulations are employed. The dependence on the experimental circumstances as target material or incoming energy on the fragment velocity is addressed later.

A major improvement of our proposed method is achieved by analysing the shape of the velocity-difference distribution Δv between neutron and fragment ($\Delta v = v_n - v_{fra}$), which is related to $R(\tau)$, instead of the shift of its mean.[3] The method can thus be used without the need of an absolute calibration of Δv to determine τ very accurately. The idea of using the ratio between delayed and prompt decays to determine the lifetime of an unbound nucleus has also been applied very recently to measure a two-proton decay lifetime [16], although the experimental technique differs from the one presented here.

To enhance the sensitivity, the target material should be chosen such that on one hand the energy loss is maximized and on the other hand the decays outside the target will happen at a considerable rate. To maximize the energy loss, target materials of large stopping power, i.e., with high density and large atomic number Z are used. This creates a box-like, broad neutron–fragment velocity difference distribution for the decays inside the target. A characteristic Δv spectrum is shown in Fig. 4. Furthermore, the target length needs to be optimized such that decays outside the target become also possible with sufficient amount. These events yield a sharp "peak" in the Δv spectrum since they as well as the neutrons do not suffer from a continuous slowing-down process in the material anymore.

2.1. Simulation for the ^{26}O case—An example

Simulation and experimental conditions are discussed in the next sections for a specific example, namely the ^{26}O ground-state decay, for which the method being developed is most sensitive to the quoted value of $\tau = 6.5$ ps [7] and well below that.

Here, the emphasis is put on illustrating the idea and describing the method. The details of the experimental realization are not described or are not even covered.

The simulations are MonteCarlo type. The code itself is tailor-made, the work flow is described in the following. With regard to Fig. 3, each ^{26}O event is produced by a one-proton removal reaction from ^{27}F in the target where the cross section and detection efficiencies are assumed to be constant as a function of reaction position as well as

energy. Secondary break-up reactions with a thick target may have a contribution of $\approx$ 10% but are not further considered here since the focus is put on presenting the method and not the experimental implementation, the ratio $R(\tau)$ is anyhow not a function of the cross section. The cross section itself is scaled to Pt according to the nuclear cross section on a C target as used in an experiment at RIBF [10]. After the reaction, as a next step, the decay point of the three-body system ^{24}O $+ 2n$ is sampled from a probability distribution which is described by an exponential-decay function with the state's proper lifetime τ as the decay constant, as given in Eq. (1). The decay itself is assumed to be a simple phase-space decay with decay energy $E_{dec} = 0$ as a good approximation [10].

The energy loss ΔE of the charged fragments and unreacted particles travelling a distance Δx in the material is calculated with JavaATIMA,[4] a program to calculate the energy loss of ions based on theory and experimental results. In addition to the used theory by Lindhard and Sørensen (applicable above 30 AMeV), it includes relevant corrections. In detail, the relation between stopping power and mean range P is defined as follows

$$\Delta x = \int_{E_0 - \Delta E}^{E_0} \left(\frac{dE}{dx}\right)^{-1} dE$$
$$= P(E_0, x_0) - P(E_0 - \Delta E, x_0 + \Delta x), \tag{11}$$

and it is evaluated from a lookup table, while the energy loss from the reaction to the decay point is, in particular, sampled stepwise in order to cope with the γ dependence of the decay curve. The knowledge of the stopping power is as important as for the DSAM for extracting the lifetime. But the absolute range of the Δv spectrum and possible peak positions allow to evaluate the quality of the underlying stopping power and can be used for calibration. The energy-loss straggling is modelled according to the relativistic Bohr formula as described in [17], whereas the effect of the angular straggling on the energy loss is found to be negligible.

Beam energy, target material, and target thickness are optimized to provide the highest sensitivity in a certain region of τ. For the lifetime to be determined with high precision, a (natural) Pt target turned out to be a good choice. Both, high mass density and large charge Z result in a large energy loss on a sufficiently short distance.

A time-of-flight resolution σ_t, assumed to be of Gaussian shape, for the neutron (fragment) measurement of 260 ps (40 ps) for a flight-path length of 11 m (9 m) are realistic values as achievable at SAMURAI setup [18] at RIBF.[5] These values were used as an input of all following simulations.

Fig. 4 shows results from a simulation as proof of principle with a well fixed incoming energy of 220 AMeV and target thickness of 6 g/cm^2 optimized to be sensitive to lifetimes around $\tau = 6.5$ ps. One identifies

---

[3] Note, in Ref. [14], e.g., Fig. 4 it is visible that the shape of the velocity difference is sensitive to the lifetime, however, the idea on using this feature is not elaborated.

[4] https://web-docs.gsi.de/~weick/atima/

[5] With the R^{3}B setup and the neutron detector NeuLAND at FAIR the time resolution will improve significantly down to $\sigma_t \lesssim 150$ ps for neutrons and $\lesssim 28$ ps for fragments [19].
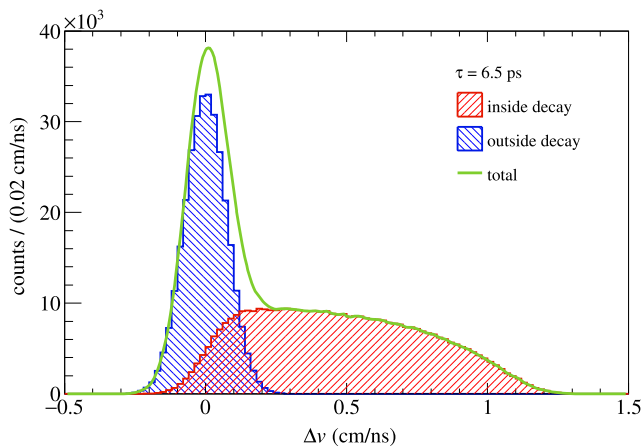
Fig. 4. (Colour online) Simulated velocity difference ($\Delta v = v_n - v_{\mathrm{fra}}$) between neutron and fragment for the ^{26}O(g.s.) decay with lifetime $\tau = 6.5$ ps; for one Pt target ($6\,\mathrm{g/cm^2}$) and incoming energy $E_{\mathrm{inc}} = 220$ AMeV. The "box shaped" contribution (red) stems from decays inside the target and the peak (blue) from outside decays.
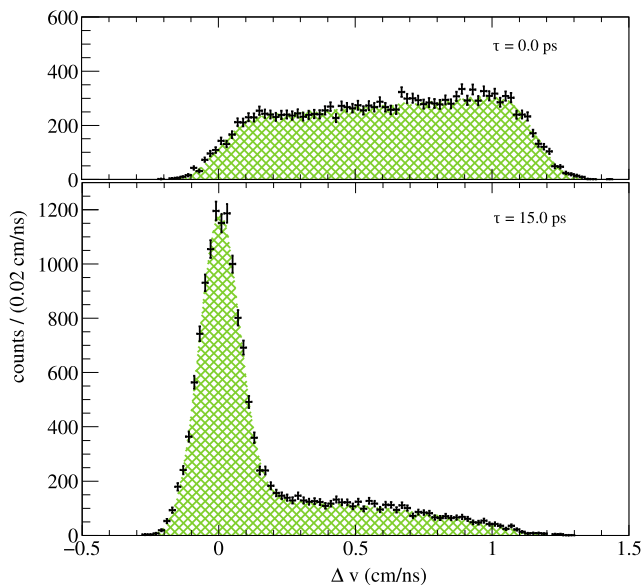

Fig. 5. (Colour online) Pseudo-experimental velocity spectra (black crosses) of 1.6×10^4 events fitted with the input-lifetime spectra (green cross-hatched) for Pt($6\,\mathrm{g/cm^2}$) and $E_{\mathrm{inc}} = 220$ AMeV. Top: $\tau = 0$ ps; bottom: $\tau = 15$ ps.

clearly two structures in the Δv spectrum of neutrons and ^{24}O fragment: a broad "box-like" shape from ~ 0 to ~ 1 cm/ns and an adjacent peak around 0 cm/ns. For prompt decays the velocity difference becomes broadest and smears out the distribution with respect to the target thickness. Again, the velocity difference of neutrons and fragment depends only on the travelled distance from the point of decay in the target, thus on τ. The charged fragment suffers from the energy loss but neutrons are insensitive. The narrow component centred around zero appears for longer lifetimes, which arises from decays outside the target with no relative energy loss between neutrons and fragments any more. The width of the narrow component is dominated by the time-of-flight resolution σ_t of the neutron detection.

2.2. Analysis procedure—determining the lifetime

As discussed above, the ratio of outside-the-target to inside-the-target decays ("box-to-peak" ratio), cf. Eq. (10), translates into the lifetime, whereas the shape of the box itself depends also slightly on τ. In order to extract the lifetime from experimental data, where τ is
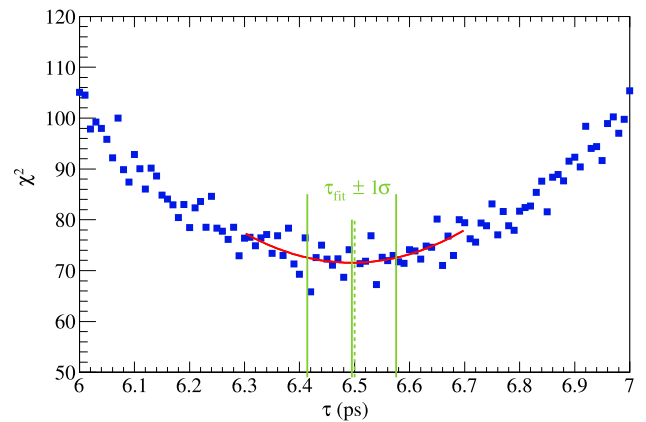

Fig. 6. (Colour online) Chi-square χ^2 distribution from the fit of trial spectra of the velocity difference Δv with lifetime τ to an assumed "experimental" spectrum, with exact lifetime $\tau = 6.5$ ps denoted by the dashed green line. The fitted minimum (red curve) indicates the deduced lifetime, depicted by the short green line, and the longer green lines confine the statistical uncertainty deduced from $\chi^2 = \chi^2_{\min} + 1$, $\tau_{\mathrm{fit}} = 6.49 \pm 0.08$ ps.

unknown, the data points are proposed to be fitted with trial spectra taken from simulations for several different lifetimes. The unnormalized chi-square χ^2 is a measure on how good the parent distribution describes the experimental data. In the following, "experimental" and simulated data are compared to test the analysis. For "experimental" spectra the simulated data are taken with reasonable but lower statistics, it is called pseudo-experimental data in the following. All the pseudo-experimental spectra are randomly filled with statistics that could be acquired within four or five days of beam time with a ^{27}F rate of 3×10^3 pps and the efficiency of triple coincidences as both is achievable at the RIBF, 1.6×10^4 events are analysed for Fig. 5.

The measured lifetime τ and the uncertainty is deduced from a second-order polynomial fit to the determined unnormalized χ^2 values around the minimum as shown in Fig. 6, where the minimum results in τ. The 1σ limit is calculated by finding the values of τ where $\chi^2 = \chi^2_{\min} + 1$ in the fit. The resulting value for the case discussed previously is $\tau = 6.49 \pm 0.08$ ps. In the following sections it is described how to increase the sensitivity.

2.3. Extended method

From known experimental results and theoretical predictions, described in Section 1, the lifetime of ^{26}O is expected to be of lower picosecond range, which is what our proposed method can measure, however the lifetime could even be smaller by orders of magnitude. In order to increase the sensitivity, the coverable lifetime range, and the luminosity within one experimental run, several targets in a row as "sandwich-like structure" are suggested in this work. Thinner targets and lower energies translate into shorter lifetimes for $R(\tau) = \mathrm{const}$. Here, the single target thicknesses are decreasing in the direction of the beam and are chosen according to energy and lifetime-sensitivity following a constant difference of the fragment flight time through the material, given as follows

$$\frac{2E + 2m_0 c^2}{\sqrt{\left(E^2 + 2Em_0 c^2\right)^3}} \Delta E = \mathrm{const}, \tag{12}$$

with the kinetic energy E and energy loss ΔE. The thickness of the initial target and incident energy are chosen such that high sensitivity is achieved for lifetimes longer than 3 ps. The target's thickness uniformity in general is of special importance. It was evaluated that deviations of $\pm 5\%$ smear out the Δv distributions so much that no result can be extracted lower than 0.5 ps that looks different than for 0 ps.

In the following, a setup of eight Pt targets with first target thickness of $3.63\,\mathrm{g/cm^2}$ and ^{27}F beam at 200 AMeV energy on target is considered. In front and behind the target stack one and two silicon detectors are
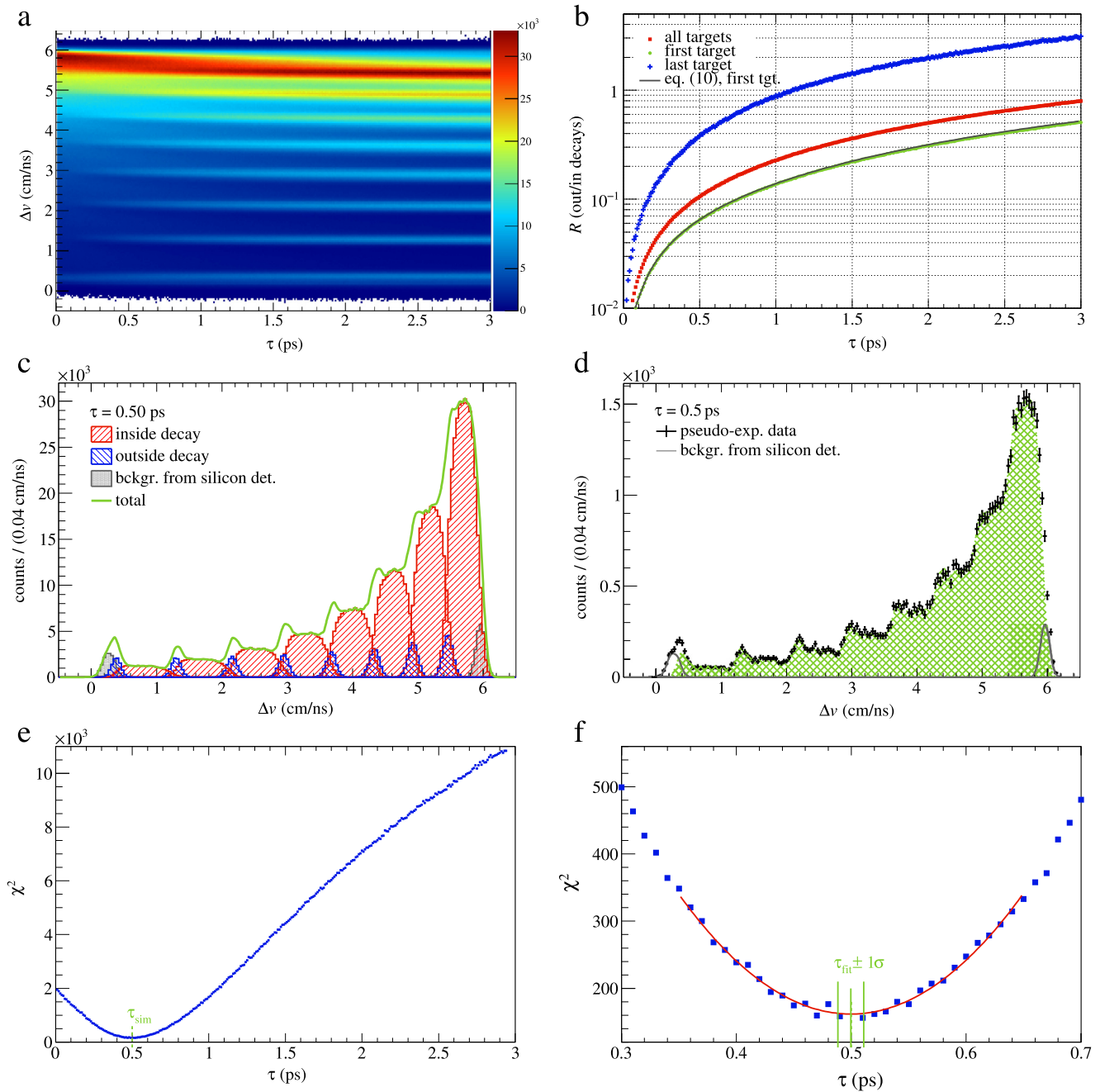
Fig. 7. (Colour online) Simulation for eight targets and optimized conditions for $\tau = 0.5$ ps and above (see text). 7(a) Velocity difference Δv as a function of the lifetime τ. The peak structure becomes more pronounced with larger lifetimes. 7(b) Inside-to-outside the target decay-ratio as function of the lifetime for only the first (green) and last target (blue) and all the simulated eight targets together (red). The "peak-to-box" ratio $R(\tau)$ increases with increasing lifetime. The simulation result is compared to the analytical Eq. (10) for the first target, for the following targets the deviation increases. 7(c) Velocity difference spectrum for $\tau = 0.5$ ps; the single components for inside (red) and outside (blue) the target decay, and the total spectrum (green) are shown. The background contribution (grey) after the ΔE cut for particle identification from the silicon detectors is included. 7(d) Fit of best trial spectrum ($\tau = 0.5$ ps, cross-hatched in green) with fixed background (grey) to pseudo-experimental data (black crosses; 6×10^4 events in total, the simulation has a factor ~ 30 more statistics) for exactly this case. 7(e) Chi-square χ^2 as function of the fit of the trial spectra with lifetime τ in steps of 0.01 ps. The green dashed lines indicates the "experimental" lifetime. 7(f) This graph shows a zoom of 7(e) in the region 0.3 ps to 0.7 ps. The fitted minimum (red curve) for $\tau_{sim} \pm 0.15$ ps indicates the deduced lifetime. The obtained lifetime $\tau_{fit} = 0.50 \pm 0.01$ ps and the 1σ uncertainty interval are denoted by the green lines.

inserted, respectively, in order to identify the proton removal reaction. In fact, these materials also act as target, see next Section 2.4. The simulation result for Δv is shown in Fig. 7(a) as function of τ in steps of 0.01 ps. For longer lifetimes the peaks of outside decays are getting more pronounced, which is also evident the ratio $R(\tau)$ in Fig. 7(b). The projection for a physical lifetime of 0.5 ps, one of the lowest reachable values, is shown in Fig. 7(c) where the sandwich-like arrangement of the targets can be recognized (cf. Fig. 3) in the repeating box-peak structure. The probed ratio of outside to inside decays is increasing from one target to another, while the targets are getting thinner and

lowering the particle's energy from one to the other. In this way, a broad range and lower lifetimes are probed as well, where the last target is most sensitive to shorter lifetimes with a distinct ratio $R(\tau = 0.5 \text{ ps}) \approx 0.38$ and a pronounced box shape. The overall Δv spectrum shows several pronounced peaks, which improves accuracy and precision of the method, even when the number of outside decays is relatively small. The first targets could also be replaced by an upstream energy degrader but sensitivity to longer lifetimes would then be lost. The approach with only one target is better suited to probe a narrow lifetime region when
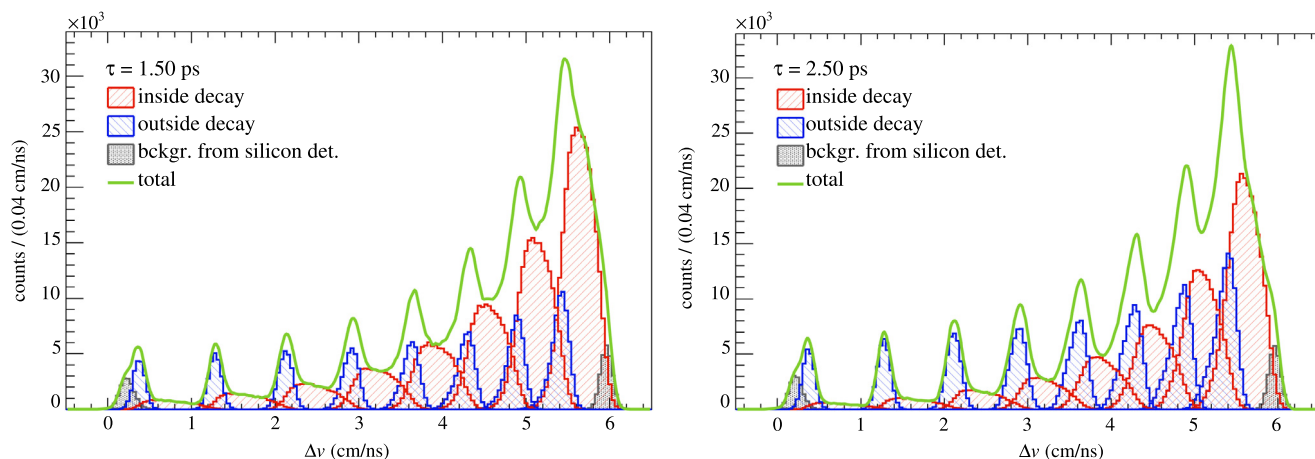
Fig. 8. (Colour online) Same as Fig. 7(c) but for $\tau = 1.5$ ps (left) and 2.5 ps (right).

the lifetime to look at is known and the setup is optimized such that the ratio $R(\tau)$ does not saturate.

It turned out that a peak-to-box ratio (outside to inside the target decays) of ~ 0.4–0.7 is optimal for deducing the lifetime with several targets. This includes a well pronounced peak and a "box" shape of the velocity-difference distribution for a certain lifetime, and for the analysis a small χ^2 value and a one-to-one relation between the extracted and simulated τ. Furthermore, the thickness is optimized such that a steep slope of the ratio $R(\tau)$ is achieved.

2.4. Contribution from auxiliary detectors

The method could be applied at one of the setups for spectroscopy of unbound neutron-rich nuclei, MoNA/NSCL [20], SAMURAI/RIBF [18], and R³B at GSI or future FAIR [19].

To identify proton removal reactions from ^{27}F, energy-loss measurements need to be conducted in front of the target stack and behind. Three simple 300 μm thick single-area silicon detectors (one in front and two behind) are proposed to be installed. Actually, it is not necessary to identify explicitly in which target the reaction happens because this is already indicated in the Δv spectrum. The targets themselves are placed sufficiently apart with 1 cm distance between them to avoid reactions in one and the decay in the following target; this covers nearly 100% for $\tau \leq 20$ ps.

A selection on incoming charge Z is applied using the first detector and in the second and third detector the outgoing charge is fixed to $Z-1$. In the simulation, the energy-loss in the detectors is treated explicitly with a resolution of $\Delta E/E = 3.5\%$ and a selection on $(Z-1) = 8$ is applied. The silicon detectors themselves act as targets (cross section scaled with $A^{1/3}$ compared to Pt) contributing to the Δv distribution as peaks at both sides of the spectrum, Fig. 7(c). The main difficulty caused by this background is that an empty target measurement will not allow to subtract the background contribution. Due to the missing energy loss in the reaction target the background from one silicon detector will overlap with the background from another detector.

This challenge can be tackled by using the information from an empty target run as input to the simulation to improve the shape of the background contribution. Also, the total amount of events which contributes to the background can be determined from the experimental data. From the known integral and the relative amplitudes of the background components they can be uniquely identified and fixed. A second approach is to use in the here discussed ^{26}O example the ^{25}O [6,9,10] reference channel as "null measurement", where the desired contributions are measured all together in the Δv spectrum, but no lifetime is expected.

The full Δv distribution is then fitted using the shapes from the simulation for several different τ, where the amplitude of the simulated

Table 1

Extracted lifetimes τ_{fit} from several analyses and their mean uncertainties in comparison with the simulated input data τ_{sim} for the examined test case with eight targets, cf. Fig. 7 & 8.

τ_{sim} (ps)	τ_{fit} (ps)	$\Delta\tau$ stat. (ps)
0.20	0.20	± 0.01
0.50	0.51	± 0.01
1.00	1.00	± 0.01
1.50	1.52	± 0.01
2.00	2.03	± 0.01
2.50	2.50	± 0.02

spectrum is the only free parameter and the background is fixed, Fig. 7(d). Here, the advantage of the target stack is that the background peaks from first and second silicon detector contribute only at the extreme edges of the Δv spectrum. Even though the last target is most sensitive to the shortest lifetimes, several peaks are present and one could also only fit the region where the silicon detectors do not contribute.

2.5. Sensitivity

The determined χ^2 is considered to be smallest in case of the real lifetime, cf. Fig. 7(e), which allows to determine the statistical uncertainty from the minimum of the χ^2 parabola as $\chi^2_{\text{min}} + 1$. The minimum number of reconstructed events in the experiment needed to determine a lifetime of 0.5 ps by a 5σ interval, only governed by the statistical uncertainty, is 5×10^3 events. In the case discussed above, the spectrum is clearly different from an instantaneous decay of a resonant ground state, see Fig. 5, which can be shown experimentally also with the one-neutron decay of ^{25}O. The method is proven to measure and confirm the neutron radioactive decay down to $\tau = 0.50 \pm 0.01$(stat) ps or even $\tau = 0.20 \pm 0.01$(stat) ps within at least a 5σ uncertainty interval under the examined conditions. Other systematic and experimental effects are not presented here. Further results from the same simulation, cf. Figs. 7 and 8, are summarized in Tab. 1.

3. Summary and outlook

We developed a method which will allow to directly measure the lifetime of neutron-unbound states from decays inside and outside the target. This method fills a gap for such decay studies and allows to measure lifetimes in the lower time regime of radioactive decays, the picosecond range. The method considers the velocity-difference spectrum between neutron(s) and fragment where the ratio of inside-to-outside decays translate into a characteristic spectrum, analysing the spectrum's

shape results in the lifetime. Thus, this method is independent of an absolute calibration of the velocity-difference spectrum.

The case of the $2n$ emitter ^{26}O was studied in detail. With a specific choice of target material and thickness according to the incoming energy we could show with simulations that the method is sensitive down to a lifetime of $\tau = 0.2$ ps within 5σ under the given conditions and statistics, especially in a target-stack arrangement. The method is however applicable to measure longer lifetimes even with one target. The systematics can be adapted for other possible candidate nuclei according to the lifetime.

Other possible candidates for neutron radioactive decays could be ^{16}B [14] or other sd-shell nuclei with a low ground-state energy and a sufficiently large angular momentum barrier.

Acknowledgements

References

[1] M. Pfützner, M. Karny, L.V. Grigorenko, K. Riisager, Radioactive decays at limits of nuclear stability, Rev. Modern Phys. 84 (2012) 567–619. http://dx.doi.org/10.1103/RevModPhys.84.567.

[2] M. Pfützner, Particle radioactivity of exotic nuclei, Physica Scripta Volume T 152 (1) (2013) 014014. http://dx.doi.org/10.1088/0031-8949/2013/T152/014014.

[3] L.V. Grigorenko, I.G. Mukha, M.V. Zhukov, Lifetime and Fragment Correlations for the Two-Neutron Decay of ^{26}O Ground State, Phys. Rev. Lett. 111 (4) (2013) 042501. http://dx.doi.org/10.1103/PhysRevLett.111.042501.

[4] M. Thoennessen, Reaching the limits of nuclear stability, Rep. Progr. Phys. 67 (2004) 1187–1232. http://dx.doi.org/10.1088/0034-4885/67/7/R04.

[5] A.H. Wapstra, IUPAC-IUPAP Transfermium Working Group, Criteria that must be satisfied for the discovery of a new chemical element to be recognized, Pure Appl. Chem. 63 (1991) 879–886. http://dx.doi.org/10.1351/pac199163060879.

[6] C. Caesar, J. Simonis, T. Adachi, Y. Aksyutina, J. Alcantara, S. Altstadt, H. Alvarez-Pol, N. Ashwood, T. Aumann, V. Avdeichikov, M. Barr, S. Beceiro, D. Bemmerer, J. Benlliure, C.A. Bertulani, K. Boretzky, M.J.G. Borge, G. Burgunder, M. Caamano, E. Casarejos, W. Catford, J. Cederkäll, S. Chakraborty, M. Chartier, L. Chulkov, D. Cortina-Gil, U. Datta Pramanik, P. Diaz Fernandez, I. Dillmann, Z. Elekes, J. Enders, O. Ershova, A. Estrade, F. Farinon, L.M. Fraile, M. Freer, M. Freudenberger, H.O.U. Fynbo, D. Galaviz, H. Geissel, R. Gernhäuser, P. Golubev, D. Gonzalez Diaz, J. Hagdahl, T. Heftrich, M. Heil, M. Heine, A. Heinz, A. Henriques, M. Holl, J.D. Holt, G. Ickert, A. Ignatov, B. Jakobsson, H.T. Johansson, B. Jonson, N. Kalantar-Nayestanaki, R. Kanungo, A. Kelic-Heil, R. Knöbel, T. Kröll, R. Krücken, J. Kurcewicz, M. Labiche, C. Langer, T. Le Bleis, R. Lemmon, O. Lepyoshkina, S. Lindberg, J. Machado, J. Marganiec, V. Maroussov, J. Menéndez, M. Mostazo, A. Movsesyan, A. Najafi, T. Nilsson, C. Nociforo, V. Panin, A. Perea, S. Pietri, R. Plag, A. Prochazka, A. Rahaman, G. Rastrepina, R. Reifarth, G. Ribeiro, M.V. Ricciardi, C. Rigollet, K. Riisager, M. Röder, D. Rossi, J. Sanchez del Rio, D. Savran, H. Scheit, A. Schwenk, H. Simon, O. Sorlin, V. Stoica, B. Streicher, J. Taylor, O. Tengblad, S. Terashima, R. Thies, Y. Togano, E. Uberseder, J. Van de Walle, P. Velho, V. Volkov, A. Wagner, F. Wamers, H. Weick, M. Weigand, C. Wheldon, G. Wilson, C. Wimmer, J.S. Winfield, P. Woods, D. Yakorev, M.V. Zhukov, A. Zilges, M. Zoric, K. Zuber, Beyond the neutron drip line: The unbound oxygen isotopes ^{25}O and ^{26}O, Phys. Rev. C 88 (3) (2013) 034313. http://dx.doi.org/10.1103/PhysRevC.88.034313.

[7] Z. Kohley, T. Baumann, D. Bazin, G. Christian, P.A. DeYoung, J.E. Finck, N. Frank, M. Jones, E. Lunderberg, B. Luther, S. Mosby, T. Nagi, J.K. Smith, J. Snyder, A. Spyrou, M. Thoennessen, Study of Two-Neutron Radioactivity in the Decay of ^{26}O, Phys. Rev. Lett. 110 (15) (2013) 152501. http://dx.doi.org/10.1103/PhysRevLett.110.152501.

[8] L.V. Grigorenko, I.G. Mukha, C. Scheidenberger, M.V. Zhukov, Two-neutron radioactivity and four-nucleon emission from exotic nuclei, Phys. Rev. C 84 (2) (2011) 021303. http://dx.doi.org/10.1103/PhysRevC.84.021303.

[9] E. Lunderberg, P.A. DeYoung, Z. Kohley, H. Attanayake, T. Baumann, D. Bazin, G. Christian, D. Divaratne, S.M. Grimes, A. Haagsma, J.E. Finck, N. Frank, B. Luther, S. Mosby, T. Nagi, G.F. Peaslee, A. Schiller, J. Snyder, A. Spyrou, M.J. Strongman, M. Thoennessen, Evidence for the Ground-State Resonance of ^{26}O, Phys. Rev. Lett. 108 (2012) 142503. http://dx.doi.org/10.1103/PhysRevLett.108.142503.

[10] Y. Kondo, T. Nakamura, R. Tanaka, R. Minakata, S. Ogoshi, N.A. Orr, N.L. Achouri, T. Aumann, H. Baba, F. Delaunay, P. Doornenbal, N. Fukuda, J. Gibelin, J.W. Hwang, N. Inabe, T. Isobe, D. Kameda, D. Kanno, S. Kim, N. Kobayashi, T. Kobayashi, T. Kubo, S. Leblond, J. Lee, F.M. Marqués, T. Motobayashi, D. Murai, T. Murakami, K. Muto, T. Nakashima, N. Nakatsuka, A. Navin, S. Nishi, H. Otsu, H. Sato, Y. Satou, Y. Shimizu, H. Suzuki, K. Takahashi, H. Takeda, S. Takeuchi, Y. Togano, A.G. Tuff, M. Vandebrouck, K. Yoneda, Nucleus ^{26}O: A Barely Unbound System beyond the Drip Line, Phys. Rev. Lett. 116 (2016) 102503. http://dx.doi.org/10.1103/PhysRevLett.116.102503.

[11] R.A. Kryger, A. Azhari, J. Brown, J. Caggiano, M. Hellström, J.H. Kelley, B.M. Sherrill, M. Steiner, M. Thoennessen, Upper limit of the lifetime of ^{16}B, Phys. Rev. C 53 (1996) 1971–1973. http://dx.doi.org/10.1103/PhysRevC.53.1971.

[12] K. Hagino, H. Sagawa, Decay dynamics of the unbound ^{25}O and ^{26}O nuclei, Phys. Rev. C 93 (2016) 034330. http://dx.doi.org/10.1103/PhysRevC.93.034330.

[13] L.V. Grigorenko, M.V. Zhukov, Continuum excitations of ^{26}O in a three-body model: 0^+ and 2^+ states, Phys. Rev. C 91 (2015) 064617. http://dx.doi.org/10.1103/PhysRevC.91.064617.

[14] M. Thoennessen, G. Christian, Z. Kohley, T. Baumann, M. Jones, J.K. Smith, J. Snyder, A. Spyrou, Novel techniques to search for neutron radioactivity, Nucl. Instrum. Methods Phys. Res. A 729 (2013) 207–211. http://dx.doi.org/10.1016/j.nima.2013.07.035.

[15] P.J. Nolan, J.F. Sharpey-Schafer, REVIEW: The measurement of the lifetimes of excited nuclear states, Rep. Progr. Phys. 42 (1979) 1–86. http://dx.doi.org/10.1088/0034-4885/42/1/001.

[16] P. Voss, T. Baumann, D. Bazin, A. Dewald, H. Iwasaki, D. Miller, A. Ratkiewicz, A. Spyrou, K. Starosta, M. Thoennessen, C. Vaman, J.A. Tostevin, ^{19}Mg two-proton decay lifetime, Phys. Rev. C 90 (2014) 014301. http://dx.doi.org/10.1103/PhysRevC.90.014301.

[17] C. Scheidenberger, H. Geissel, H.H. Mikkelsen, F. Nickel, S. Czajkowski, H. Folger, H. Irnich, G. Münzenberg, W. Schwab, T. Stöhlker, T. Suzuki, B. Voss, Energy-Loss-Straggling Experiments with Relativistic Heavy Ions in Solids, Phys. Rev. Lett. 77 (1996) 3987–3990. http://dx.doi.org/10.1103/PhysRevLett.77.3987.

[18] T. Kobayashi, N. Chiga, T. Isobe, Y. Kondo, T. Kubo, K. Kusaka, T. Motobayashi, T. Nakamura, J. Ohnishi, H. Okuno, H. Otsu, T. Sako, Y. Shimizu, K. Sekiguchi, K. Takahashi, R. Tanaka, K. Yoneda, SAMURAI spectrometer for RI beam experiments, Nucl. Instrum. Methods Phys. Res. B (ISSN: 0168-583X) 317 (Part B) (2013) 294–304. http://dx.doi.org/10.1016/j.nimb.2013.05.089.

[19] R^{3}B Collaboration, Technical Proposal for the Design, Construction, Commissioning and Operation of R^{3}B, 2005.

[20] T. Baumann, J. Boike, J. Brown, M. Bullinger, J.P. Bychoswki, S. Clark, K. Daum, P.A. Deyoung, J.V. Evans, J. Finck, N. Frank, A. Grant, J. Hinnefeld, G.W. Hitt, R.H. Howes, B. Isselhardt, K.W. Kemper, J. Longacre, Y. Lu, B. Luther, S.T. Marley, D. McCollum, E. McDonald, U. Onwuemene, P.V. Pancella, G.F. Peaslee, W.A. Peters, M. Rajabali, J. Robertson, W.F. Rogers, S.L. Tabor, M. Thoennessen, E. Tryggestad, R.E. Turner, P.J. Vanwylen, N. Walker, Construction of a modular large-area neutron detector for the NSCL, Nucl. Instrum. Methods A 543 (2005) 517–527. http://dx.doi.org/10.1016/j.nima.2004.12.020.